Available online at www.sciencedirect.com
SCIENCE DIRECT®
International Journal of Heat and Mass Transfer 49 (2006) 2810–2819
International Journal of HEAT and MASS TRANSFER
www.elsevier.com/locate/ijhmt

Determination of the anisotropic radiative properties of a porous material by radiative distribution function identification (RDFI)

Barbar Zeghondy, Estelle Iacona *, Jean Taine

Laboratoire EM2C, École Centrale Paris, Grande Voie des Vignes – 92295 Châtenay Malabry, France

Received 12 October 2005; received in revised form 9 February 2006
Available online 27 April 2006

Abstract

The anisotropic extinction and absorption coefficients of a high porosity material with a semi-transparent solid phase are directly obtained from identification of the statistical cumulated distribution function of extinction distances in the material, linked to that of the chords, and the corresponding function in the equivalent semi transparent medium. The bidirectional phase function is then determined without any hypothesis. The model only requires the knowledge of the material morphology, given by a X-ray tomography and the phases local radiative properties.

Keywords: Radiation; Porous media; Multi scale approach; Extinction; Scattering; Phase function

1. Introduction

Accurate calculations of radiative transfer in porous media are required in many applications such as catalytic combustion, thermal shields, nuclear safety of corium, fuel cells (SOFC), etc. The characterization of the radiative properties of these media is a key point for these calculations. Most of the characterization methods are based on the identification of parameters, such as absorption and scattering coefficients and the parameters of a phase function of an assumed type. This identification is carried out between reference results, issued from experiments or calculations, and results issued from a given transfer model. Consequently, the identified parameters often depend on the chosen radiative transfer model.

Works based on identification methods applied to porous media and using calculated reference results are first presented. An identification of absorption and scattering coefficients of randomly packed beds of uniform diameter spheres has been carried out by Yang et al. [1]. In this work, the transmittance and reflectance have been calculated by a reference Monte Carlo transfer model and by a two flux transfer model for the semi-transparent equivalent medium. Argento and Bouvard [2] have developed similar works using ray tracing calculations as reference. Subramaniam and Mengüc [3] have determined from a Monte Carlo method, for a medium of known extinction coefficient, both the albedo and the asymmetry parameter g by assuming the type of phase function. Also for packed beds of spheres, Singh and Kaviany [4,5] have taken into account the screen effect by phenomenological scaling factors applied to additive absorption and scattering coefficients calculated from the Mie theory. The reference results are issued from reflectance and transmittance calculations by a Monte Carlo approach. Fu et al. [6] have identified the extinction coefficient and the albedo of a set of spheres from reflectance and transmittance data obtained both by a reference calculation based on a unit cell model and a zonal approach, and by a discrete ordinate method using an isotropic scattering phase function of a given type. Coquard and Baillis [7–9] have also taken into account the screen effect of a packed bed of semi-transparent spheres, of optical index assumed equal to the propagation medium index. They have used a Monte Carlo technique to directly compute the collimated intensity and obtained the extinction

* Corresponding author. Tel.: +33 141131075; fax: +33 147028035.
E-mail address: estelle.iacona@em2c.ecp.fr (E. Iacona).

0017-9310/$ - see front matter © 2006 Elsevier Ltd. All rights reserved.
doi:10.1016/j.ijheatmasstransfer.2006.02.034

coefficient. The albedo and the phase function parameters have been identified from emerging intensity data obtained both by a reference model using a Monte Carlo technique and by a discrete ordinate model. Brewster [10] has developed a simple model, based on a mean extinction distance, in order to compute the extinction coefficient of a packed bed by taking into account the particle volume effect.

Other identification methods are based on reference measurements. Glicksman et al. [11] have measured the directional transmissivity of foam and glass fiber by using a CO_2 laser. They have identified absorption and extinction coefficients and phase function from simple solutions of the RTE equation. Hendricks and Howell [12,13] have experimentally determined hemispherical reflectance and transmittance of high porosity ceramics and of sets of opaque identical spheres randomly distributed. For both media, absorption and scattering coefficients and different types of phase functions have been identified by using a discrete ordinate transfer methods. The same authors [14] have also developed a new radiative analysis approach, based on the previous reference and transfer method, applied to reticulated porous ceramics. In this approach, the direct transmittance is treated separately from the transmittance issued from interactions with internal structures. Baillis-Doermann et al. [15–18] have carried out similar works for open cell foam insulation. The originality of these works is to use predicted expressions of absorption and extinction coefficients from simple geometrical calculations. These expressions depend on the local opaque medium reflectivity which is identified, as the phase function parameters, by a technique similar to those of Refs. [12–14]. The characterization of radiative properties of dispersed media is also reviewed in Ref. [19].

In all the previously cited approaches, the absorption and extinction coefficients and the phase function of a medium equivalent to the porous medium have been identified from global radiative data, such as transmittance or reflectance measurements or calculations, and by using a given radiative transfer model for a system (slab, cylinder,...). Tancrez and Taine [20] have determined the same type of radiative properties directly from their local definitions, linked to the definition itself of a semi-transparent medium, i.e. independently of any radiative transfer model. A direct general determination method of the scattering and absorption coefficients and of the phase function of high porosity media, with a transparent fluid phase and an opaque solid phase, has been developed. It is valid for wavelengths which are small compared to the typical structure length, so that diffraction is negligible. The method has been applied to virtual statistically isotropic and homogeneous media. The absorption and extinction coefficients are obtained from both the morphological properties of the porous media and the local radiative properties of the opaque solid phase by radiative distribution function identification (RDFI). In this method, the cumulated distribution functions of extinction and absorption of the real porous medium obtained by a stochastical Monte Carlo method are identified with the corresponding cumulated functions in the equivalent continuous semi-transparent model. It has been established in Ref. [20] that for a porosity higher than 0.65, the extinction and absorption coefficients β and κ_v are accurately obtained.

The aim of the present paper is to generalize the RDFI method to a porous medium with a solid semi-transparent phase and to implement it for a real porous medium, which is also statistically anisotropic. The morphology of this porous medium has been obtained by a monochromatic X-ray tomography at the European Synchrotron Radiation Facility (ESRF).

In Section 2, the generalized RDFI method is presented. Its aim is to determine the extinction and absorption coefficients of the equivalent semi-transparent medium, depending on direction of the incident rays and the associated phase function. A key point of the method, the characterization of the interfacial impacts of rays used in the Monte Carlo approach, is discussed in Section 3. The method has been eventually applied to a mullite sample and the results are presented in the last Section.

2. Generalized RDFI method

First, the approach of Ref. [20] is briefly summarized. It is generalized then to a porous medium with a semi-transparent solid phase, for the determination of the extinction and absorption coefficients and the phase function of an equivalent semi-transparent continuous medium.

A radiative distribution function identification (RDFI) method has been applied to a porous medium with a transparent fluid phase and an opaque solid phase in Ref. [20]. It is based on a statistical formulation of the physical laws of radiation. The main idea is to determine the extinction coefficient β of a continuous semi transparent medium equivalent to the porous medium by identification of the extinction cumulated distribution function $G_e(s)$ of the real porous medium with the corresponding extinction distribution function of the semi-transparent medium $g_e(s)$ equal to $1-\exp(-\beta s)$ by a least square fit method. The same identification is made between the real porous medium absorption cumulated function $G_a(s)$ and the equivalent medium absorption cumulated function $p_a(s)$ equal to $\kappa_v/\beta[1-\exp(-\beta s)]$ to obtain κ_v, absorption coefficient of the equivalent medium. s is the current distance in the equivalent semi-transparent medium. As detailed in Ref. [20] (see Fig 1.a. of this Ref.), $G_e(s)$ is in fact the cumulated distribution function of the distance between a current point M of the fluid phase and its impact point I on the solid phase along a ray. Each impact of a ray corresponds to an absorption or a reflection phenomenon, i.e. to extinction as shown in Fig. 1a. $G_a(s)$ is then associated with the absorption at the impact point I. In practice, $G_e(s)$ and $G_a(s)$ are calculated by using a Monte Carlo approach and by generating a huge set of rays from any current point M of the fluid phase. The identifications between $G_e(s)$ and $g_e(s)$, and $G_a(s)$ and $p_a(s)$ are carried out for an optical thickness βs in the range $[0,3]$, of interest for a semi-transparent medium.

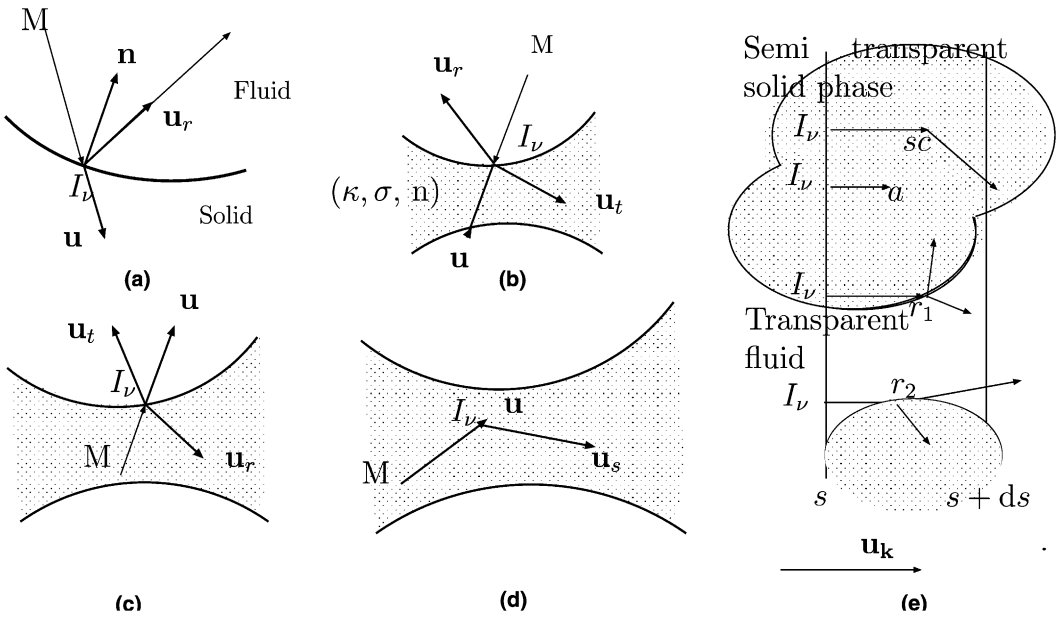

Fig. 1. Reflection, transmission and scattering configurations: (a) opaque solid phase; (b,c,d) semi-transparent solid phase; (e) different events in a slab s, $s + ds$ for an incident intensity I_ν in the normal direction $\mathbf{u_k}$; *sc* and *a* represent scattered and absorbed rays in the solid phase; r_1 and r_2 scattered rays at the interface.

The scattering phase function $p_\nu(\mathbf{u}, \mathbf{u_r})$ of the equivalent semi-transparent medium is directly calculated as the distribution function associated with the probability that, in the spherical frame of axis $\mathbf{u}$, the reflected ray belongs to an elementary solid angle $d\Omega(\mathbf{u}_r)$, depending on the interface reflection law.

We now consider the identification of the extinction and absorption coefficients β_ν and κ_ν and the phase function $p_\nu(\mathbf{u}, \mathbf{u}')$ of a unique semi-transparent medium associated with a statistically anisotropic porous medium with a transparent fluid phase and a semi-transparent solid phase. As previously, an originality of the method is to identify β_ν, κ_ν and p_ν directly from their definitions. But an important difference is that the rays to be considered are issued from current points M belonging to both the fluid and the solid phases.

The solid phase is now characterized by an optical index n, absorption and scattering coefficients $\kappa_{S\nu}$ and $\sigma_{S\nu}$ and a phase function $p_{S\nu}$.

2.1. Establishment of the equivalent RTE

In this subsection, the use of a radiative transfer equation (RTE) for a unique equivalent semi-transparent medium associated with a porous medium with a fluid phase 1 and a solid phase 2 is justified. Two coupled specific RTE can be written for these phases, where Π_i is the volume fraction of the phase i ($\Pi_1 = \Pi, \Pi_2 = 1 - \Pi$); $I_{i\nu}(\mathbf{u})$ the incident intensity in the current solid angle $d\Omega$ within the phase i; n_i, $\beta_{i\nu}$, $\kappa_{i\nu}$ the optical index and the extinction and absorption coefficients of this phase; $\sigma_{ii\nu}$ the partial scattering coefficient of the phase i associated with: (i) partial reflection of $I_{i\nu}(\mathbf{u}')$ at the interface inside this phase, as shown in Fig. 1b and c; (ii) partial scattering of $I_{i\nu}(\mathbf{u}')$ inside a semi-transparent phase, as shown in Fig. 1d; $p_{ii\nu}(\mathbf{u}, \mathbf{u}')$ the phase function associated with $\sigma_{ii\nu}$; $\sigma_{ji\nu}$ the partial scattering coefficient of the phase j associated with the partial transmission of $I_{j\nu}(\mathbf{u}')$ from the phase j to the phase i through the interface, as shown in Fig. 1b and c; $p_{ji\nu}(\mathbf{u}, \mathbf{u}')$ the associated phase function. The terms containing $\sigma_{ji\nu}$ couple the RTEs.

$$\Pi_i \frac{dI_{i\nu}(\mathbf{u})}{ds} + \Pi_i \beta_{i\nu} I_{i\nu}(\mathbf{u}) = \Pi_i n_i^2 \kappa_{i\nu} I_\nu^\circ(T_i) + \Pi_i \frac{\sigma_{ii\nu}}{4\pi} \int_{4\pi} p_{ii\nu}(\mathbf{u}, \mathbf{u}') I_{i\nu}(\mathbf{u}') d\Omega' + \Pi_j \frac{\sigma_{ji\nu}}{4\pi} \int_{4\pi} p_{ji\nu}(\mathbf{u}, \mathbf{u}') I_{j\nu}(\mathbf{u}') d\Omega', \quad i, j = 1, 2;\ i \neq j \tag{1}$$

In the model considered here, based on a unique RTE for the whole porous medium, an assumption is required in order to define the unique intensity I_ν in the current solid angle $d\Omega$. We assume that I_ν is an effective intensity

$$I_\nu(\mathbf{u}) = I_{1\nu}(\mathbf{u}) = I_{2\nu}(\mathbf{u}). \tag{2}$$

From Eqs. (1) and (2), we obtain the whole porous medium RTE

$$\frac{dI_\nu(\mathbf{u})}{ds} + \beta_\nu I_\nu(\mathbf{u}) = n_{\text{eff}}^2 \kappa_\nu I_\nu^\circ(T) + \frac{\sigma_\nu}{4\pi} \int_{4\pi} p_\nu(\mathbf{u}, \mathbf{u}') I_\nu(\mathbf{u}') d\Omega' \tag{3}$$

in which appear the equivalent coefficients X_ν equal to $\Pi X_{1\nu} + (1 - \Pi) X_{2\nu}$, where the $X_{i\nu}$ designate $\kappa_{i\nu}$ and $\beta_{i\nu}$. The phase function p_ν is given by

$$p_\nu(\mathbf{u}, \mathbf{u}') = \sigma_\nu^{-1} \{ \Pi [p_{11\nu}(\mathbf{u}, \mathbf{u}') \sigma_{11\nu} + p_{12\nu}(\mathbf{u}, \mathbf{u}') \sigma_{12\nu}] + (1 - \Pi) [p_{22\nu}(\mathbf{u}, \mathbf{u}') \sigma_{22\nu} + p_{21\nu}(\mathbf{u}, \mathbf{u}') \sigma_{21\nu}] \}. \tag{4}$$

By following the arguments (i) and (ii) of the previous discussion, we can write:

$$p_{22\nu}(\mathbf{u},\mathbf{u}')\sigma_{22\nu} = p_{22\nu}^{\mathrm{refl}}(\mathbf{u},\mathbf{u}')\sigma_{22\nu}^{\mathrm{refl}} + p_{S\nu}(\mathbf{u},\mathbf{u}')\sigma_{S\nu}, \tag{5}$$

where $p_{22\nu}^{\mathrm{refl}}(\mathbf{u},\mathbf{u}')\sigma_{22\nu}^{\mathrm{refl}}$ corresponds to the internal interfacial reflection and $p_{S\nu}(\mathbf{u},\mathbf{u}')\sigma_{S\nu}$ to the real scattering in the volume of the solid phase. The effective optical index n_{eff} is equal to

$$n_{\mathrm{eff}\nu}^2\kappa_\nu = \Pi n_1^2\kappa_{1\nu} + (1-\Pi)n_2^2\kappa_{2\nu}. \tag{6}$$

The phase 1 is here transparent, $\Pi n_1^2\kappa_{1\nu}$ vanishes and $n_{\mathrm{eff}\nu}$ is equal to n.

In the following, all the radiative properties of the equivalent semi transparent medium β_ν, κ_ν and p_ν are determined by the RDFI method.

2.2. Extinction and absorption coefficients

In the generalized method, absorption occurs within the solid phase and different phenomena which occur in the porous medium are modeled as scattering in the equivalent continuous medium: reflection and transmission at the interface between the two phases and scattering into the solid phase here also modeled as semi-transparent. In any case, extinction by scattering and absorption is stochastically modeled from the distribution function of the distance MI of a current ray from a source point M to an extinction point I, where it vanishes. Indeed all the types of extinction phenomena are associated with the following set of events: (i) if M is in the transparent fluid phase, the ray vanishes once it impacts the solid phase at the point I of the interface, as shown in Fig. 1b; (ii) if M is in the semi-transparent solid phase, it vanishes by two ways, by impacting the interface at the point I as shown in Fig. 1c or by extinction at the point I of the solid semi-transparent phase, i.e. by scattering or absorption, as shown in Fig. 1d. These phenomena depend both on the porous medium geometry and on the local radiative properties of the solid phase. All these absorption and scattering phenomena are also summarized in Fig. 1e, for an elementary interval s, $s+\mathrm{d}s$ of the porous medium normal to the $\mathbf{u_k}$ direction of the incident intensity I_ν. In these conditions, in the Monte Carlo approach applied to the local scale of the porous medium, the extinction cumulated distribution function associated with a given direction of unit vector $\mathbf{u_k}$ is equal to the cumulated distribution function of the length MI, i.e.

$$G_{\mathrm{e}}(s,\mathbf{u_k}) = \frac{1}{V}\frac{1}{\Delta\Omega_k}\int_0^s\int_V\int_{\Delta\Omega_k}\delta[s'-s_0(\mathbf{r},\mathbf{u})]\,\mathrm{d}\Omega(\mathbf{u})\,\mathrm{d}\mathbf{r}\,\mathrm{d}s', \tag{7}$$

where s is the current distance from the source point M along the current ray, of unit vector $\mathbf{u}$ and elementary solid angle $\mathrm{d}\Omega(\mathbf{u})$; $s_0(r,\mathbf{u})$ the distance from M to the extinction point I at the interface or within the semi-transparent solid phase as previously explained; $\Delta\Omega_k(\mathbf{u_k})$ a discretized solid angle; δ the Dirac function. The summation is carried out on the whole volume of the porous medium V, with the same weight for each elementary volume of the two phases; it is a consequence of the discussion of the introduction of Section 2.

In the continuous medium approach, the extinction is simply characterized by $\beta_\nu(\mathbf{u_k})$ and the cumulated extinction distribution function

$$g_{\mathrm{e}}(s,\mathbf{u_k}) = 1-\exp[-\beta_\nu(\mathbf{u_k})s]. \tag{8}$$

As in Ref. [20], $\beta_\nu(\mathbf{u_k})$ is determined by identification of $G_{\mathrm{e}}(s,\mathbf{u_k})$ and $g_{\mathrm{e}}(s,\mathbf{u_k})$ by a least square fit method. The validity range of this identification can be deduced from the relative error function $\epsilon_{\mathrm{e}}(\beta_\nu)$, i.e.

$$\epsilon_{\mathrm{e}}(\beta_\nu) = \left\{\sum_{i=0}^{N}[G_{\mathrm{e}}(s_i,\mathbf{u_k})-g_{\mathrm{e}}(s_i,\mathbf{u_k})]^2 \Big/ \sum_{i=0}^{N}[1-G_{\mathrm{e}}(s_i,\mathbf{u_k})]^2\right\}^{1/2}, \tag{9}$$

where s_i are discretized values of s in the range $[0,3]$ of βs.

As previously explained, absorption only occurs in the semi-transparent solid phase. The probability of absorption by the porous medium between the distances s and $s+\mathrm{d}s$ from a source point M is written

$$\mathrm{d}G_{\mathrm{a}}(s,\mathbf{u_k}) = \frac{1}{V}\frac{1}{\Delta\Omega_k}\,\mathrm{d}s\int_{V_S}\int_{\Delta\Omega_k}\kappa_{\nu S}\delta[s-s_0(\mathbf{r},\mathbf{u})]\,\mathrm{d}\Omega(\mathbf{u})\,\mathrm{d}\mathbf{r}, \tag{10}$$

where $\kappa_{\nu S}$ is the absorption coefficient of the semi-transparent solid phase; $s_0(\mathbf{r},\mathbf{u})$ is now the distance from M to an absorption point I within the solid phase. It is worth noticing that the sum in Eq. (10) is only carried out for the volume V_S of the solid phase. The normalization by the volume V of the whole medium allows us to implicitly take into account the porosity of the medium as discussed in the introduction of Section 2. The corresponding probability of absorption for the equivalent continuous medium model, $\mathrm{d}p_{\mathrm{a}}(s,\mathbf{u_k})$ is

$$\mathrm{d}p_{\mathrm{a}}(s,\mathbf{u_k}) = \exp[-\beta_\nu(\mathbf{u_k})s]\kappa_\nu(\mathbf{u_k})\,\mathrm{d}s, \tag{11}$$

where $\kappa_\nu(\mathbf{u_k})$ is the continuous medium absorption coefficient determined by identification of the cumulated absorption probability $G_{\mathrm{a}}^*(s,\mathbf{u_k})$, i.e.

$$G_{\mathrm{a}}^*(s,\mathbf{u_k}) = \int_s^\infty \mathrm{d}G_{\mathrm{a}}(s,\mathbf{u_k}) \tag{12}$$

with the corresponding sum of Eq. (11), i.e. $\kappa_\nu/\beta_\nu\exp(-\beta_\nu s)$, with an identification relative error function $\epsilon_{\mathrm{a}}(\kappa_\nu)$,

$$\epsilon_{\mathrm{a}}(\kappa_\nu) = \left\{\sum_{i=0}^{N}[G_{\mathrm{a}}(s_i,\mathbf{u_k})-p_{\mathrm{a}}(s_i,\mathbf{u_k})]^2 \Big/ \sum_{i=0}^{N}[G_{\mathrm{a}}(s_i,\mathbf{u_k})]^2\right\}^{1/2}. \tag{13}$$

2.3. Phase function

For an opaque solid phase, the phase function of the equivalent medium is only due to the reflection at the

interface between the two phases of the porous medium as shown in Fig. 1a. Its expression, given in Ref. [20], is

$$\frac{p_v(\mathbf{u},\mathbf{u_r})}{4\pi}\,\mathrm{d}\Omega_r(\mathbf{u_r}) = \frac{\mathrm{d}\Omega_r(\mathbf{u_r})\int_{V_F}\rho_v''[\mathbf{u},\mathbf{u_r},\mathbf{n}(\mathbf{u},\mathbf{r})]\mathbf{u}\cdot\mathbf{n}(\mathbf{u},\mathbf{r})(\mathrm{d}\mathbf{r}/V_F)}{\int_{\Delta\Omega}\int_{V_F}\rho_v''[\mathbf{u},\mathbf{u_r},\mathbf{n}(\mathbf{u},\mathbf{r})]\mathbf{u}\cdot\mathbf{n}(\mathbf{u},\mathbf{r})(\mathrm{d}\mathbf{r}/V_F)\,\mathrm{d}\Omega_r(\mathbf{u_r})} \quad (14)$$

with $\rho_v''[\mathbf{u},\mathbf{u_r},\mathbf{n}(\mathbf{u},\mathbf{r})]$ the bidirectional reflectivity defined by Siegel and Howell [21], $\mathbf{u}$, $\mathbf{u_r}$ the unit vectors of the incident and reflected rays shown in Fig. 1e. Let us briefly comment this equation. The direction $\mathbf{u}$ of the incident ray is given. In practice, the sum over V_F corresponds to random choices of a source points $M(\mathbf{r})$ within the fluid phase. Consequently, the impact point I is determined, which leads to the normal unit vector $\mathbf{n}$ depending on $\mathbf{u}$ and $\mathbf{r}$.

In fact, in our case, there are now five types of contributions to the global phase function of the equivalent semi-transparent medium i.e. p_{11v}, p_{12v}, p_{21v}, p_{22v}^{refl} and p_{Sv} introduced in Eqs. (4) and (5). Let us remember that in these expressions, the index 1 refers to the fluid phase and the index 2 to the solid phase. The expressions of p_{11v} and p_{22v}^{refl} which deal with internal reflection in fluid and solid phases respectively, are similar to that of p_v in Eq. (14); $\rho_v''[\mathbf{u},\ \mathbf{u_r},\ \mathbf{n}(\mathbf{u},\mathbf{r})]$ is now the interfacial bidirectional reflectivity. The sum is carried out on V_S instead of V_F for p_{22v}^{refl}. The expression of p_{12v} is deduced from Eq. (14) by replacing $\mathbf{u_r}$ by $\mathbf{u_t}$ and the reflectivity $\rho_v''[\mathbf{u},\ \mathbf{u_r},\ \mathbf{n}(\mathbf{u},\mathbf{r})]$ by the interfacial transmissivity $\tau_v''[\mathbf{u},\ \mathbf{u_t},\ \mathbf{n}(\mathbf{u},\ \mathbf{r})]$. In the case of p_{21v}, the sum on V_F is moreover replaced by a sum on V_S. Under the assumption of an optically smooth interface for the considered radiation wavelength, the bidirectional interfacial reflectivity ρ_v'' and transmissivity τ_v'' are calculated by using the Descartes law depending on the optical index of the two media, given for instance in Ref. [22]. But, more general expressions of ρ_v'' and τ_v'' can be used to take into account effects of interface roughness at a small spatial scale, which is not included in the morphological definition of the material.

3. Characterization of the interfacial impacts of the rays

In practice, the morphological properties of a real porous medium are often issued from a X-ray tomography and defined as a tridimensional set of voxel intensities associated with the tomography technique in use. In these conditions, the aim of this section is to define how to obtain, in the RDFI method, both the location of the impact point I of a current ray MI at the interface between the two phases, and the normal vector at this interface at the point I. The aim of this section is to discuss the validity of the determination of I in the case of a simulated tomography of a virtual statistically isotropic porous medium.

The virtual medium is a set of dispersed overlapping transparent spheres (DOTS) in a solid opaque phase as defined in Ref. [20]. As this type of media has been extensively studied in this last paper, its results are here considered as references. The reference case is a set of DOTS characterized by a porosity Π of 0.8 and a Gaussian radius distribution $R_i = r(1+\delta x)$ where r is the mean value of $\langle R_i\rangle$, x the normalized Gaussian variable and δ the standard deviation equal to 0.25.

The studied virtual medium is divided into n^3 cubic voxels of edge a. In the considered simulation, each voxel has numerically been characterized by a digitalized intensity level in the range $[0,255]$ equal to the integer part of $255(1-\Pi_V)$, where Π_V is the voxel porosity, of which calculation is detailed in Ref. [23]. The key parameter of this study is the resolution parameter D/a, where D is the mean pore diameter. The interface, determined by the simulation, is defined as a surface Σ_t characterized by a given threshold intensity value I_t, which has to be chosen consistent with the medium porosity Π. Any voxel characterized by an intensity bigger (smaller) than the threshold is then considered in the solid (fluid) phase. The simulated interface is defined by a marching cube algorithm [24,25], which is based on the interpolation of the positions of the triangle vertices defining the isosurface Σ_t in a cube built with 8 voxels of the tomography.

After this step, the general Monte Carlo approach of Ref. [20] has been applied. The extinction coefficients values of the simulation are compared with the corresponding results directly obtained in Ref. [20] in Fig. 2a. The accuracy of the determination of G_e is characterized by a standard deviation criterion σ_{MC} defined as

$$\sigma_{MC} = \left\{\sum_j [G_{ei+1}(s_j) - G_{ei}(s_j)]^2\right\}^{1/2}, \quad (15)$$

where the index i deals with the successive sets of rays in use in the Monte Carlo calculation. In Eq. (15), the $i+1$th set of rays contains ten times more rays than the ith set. σ_{MC} is typically equal to 2×10^{-3} for 10^6 rays. The parameter $\epsilon_e(\beta)$ which characterizes the identification error of G_e and g_e, defined by Eq. (9), is equal to 1.5×10^{-2}. The influence of the choices of I_t and D/a on the identified radiative properties are shown in Fig. 2a and b. For instance, it appears in Fig. 2a that, for D/a close to 10, the relative error ϵ between the reference value of β and the corresponding value issued from the simulation is minimal and less than 3×10^{-3}, for a threshold intensity close to 180. It is worth noticing that this threshold intensity value used in the simulation leads to the virtual medium porosity. Fig. 2b will be used to define the requirement of the tomography in the next Section. The accuracy of the determination of the normals by the marching cube approach can be estimated by the comparison of the distribution function $F(\mu_i)$ of μ_i the cosine of the incidence angle, obtained from both the marching cube method and the reference analytical calculations of Tancrez and Taine [20]. Indeed the phase function only depends on $F(\mu_i)$ and on the reflection law. Typical results are shown in Fig. 2c; they agree for all the range $[0;1]$ of μ_i values.

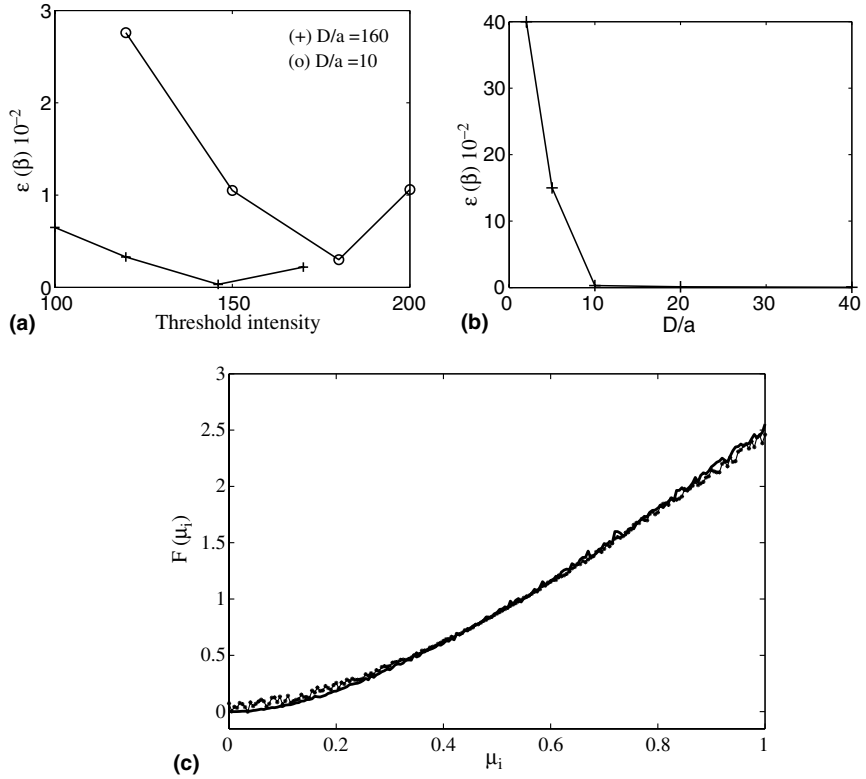

Fig. 2. (a) Relative error $\epsilon = (\beta_{ref} - \beta_{simul})/\beta_{ref}$ vs the threshold intensity and the resolution parameter D/a: $\Pi = 0.8$; Gaussian distribution. (b) Minimum relative error $\epsilon = (\beta_{ref} - \beta_{simul})/\beta_{ref}$ vs the resolution parameter D/a: $\Pi = 0.8$; Gaussian distribution. (c) Distribution function of the incidence angle cosine $F(\mu_i)$ calculated: — analytically as in Ref. [20], (+) by the marching cube method. $D/a = 160$; $\Pi = 0.8$; DOTS.

4. Application to a real anisotropic porous material

4.1. Studied material

The material is a mullite foam of EcoCeramics, Netherlands, of porosity 0.85, used in foam burners. It is characterized by three scales of porosity, the smallest ones have been determined by a mercury porosimetry as shown in Fig. 3. The corresponding typical pore sizes are 1 and 40 μm. The typical largest pore size, non-measurable by this technique, is 300 μm. The interest of this material, reason of its choice, is that the three ranges of the pore distribution do not overlap; three partial porosities 0.40, 0.11 and 0.34 can be crudely associated with the typical pore sizes 1, 40 and 300 μm, respectively.

The local radiative properties of the solid phase, associated with only the 1 μm pores, have been experimentally determined by Zeghondy et al. [26] for the 0.6328 μm wavelength. Consequently, we have not to take them into account in the Monte Carlo spatial model. The values of the real index n, the extinction coefficient β_S and the albedo ω_S determined in Ref. [26] are 1.48, 105 mm^{-1} and 0.993, respectively. The phase function of the sample is, in the following, assumed to be isotropic ($p_{Sv} = 1$). This assumption has been justified in the sensitivity study to the phase function in Section 3.2. of Ref. [26]. It is worth of noticing that the typical element of the solid phase of about 0.08 to 0.1 mm. The corresponding extinction thickness is of about 10 which is of the same order of magnitude as the solid sample optical thickness. In both cases, the materials are in the thick optical thickness limit.

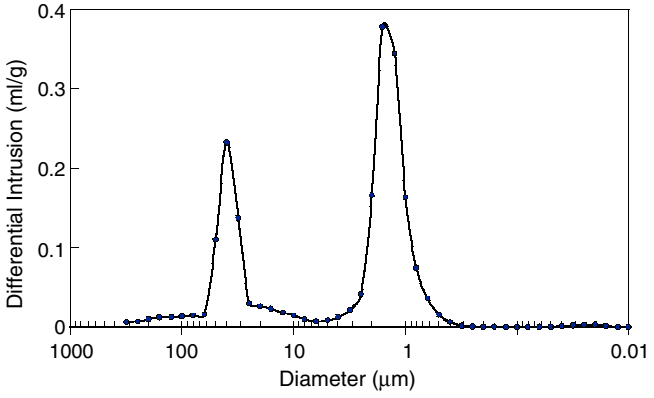

Fig. 3. Differential intrusion results measured by mercury porosimetry.

The bidirectional transmissivity τ_v'' and reflectivity ρ'' defined in Section 2.3 have been calculated with the Descartes law [22], i.e. by considered the interface as optically smooth. The effect of the interface roughness is discussed in Ref. [26]. The dimensions of the sample to be tomographed have been chosen from a simple analysis. The largest distance to be accounted for in the cumulated distribution function G_e is linked to the largest pore sizes. If the medium

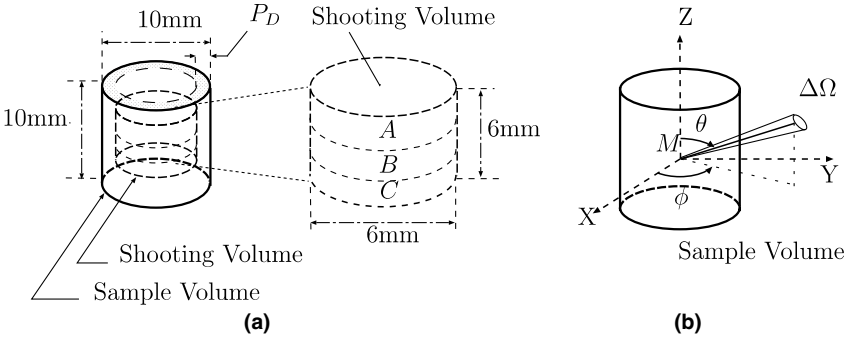

Fig. 4. (a) Tomographed sample and shooting volumes A, B and C; (b) spherical coordinates according to the sample axes, M is a current original point inside a shooting volume.

is crudely modeled by a set of dispersed overlapping transparent spheres of 300 μm mean pore diameter $\overline{D}$, the critical length s_c, corresponding to an optical thickness of 3, is a function of the porosity Π and $\overline{D}$, i.e. $s_c = -0.8\overline{D}/[\ln(1-\Pi)(\Pi^{-1}-1)]$ as established in Ref. [20]. s_c is then about 1 mm. From this analysis the dimensions have been chosen sufficiently large in order to: (i) avoid boundary effects associated with possible downgraded pores close to the boundary; (ii) allow us to characterize the spatial homogeneity of the medium. Consequently, we have chosen to tomograph a cylindrical sample of 10 mm diameter and 10 mm height, shown in Fig. 4a.

A key point is to choose a spatial resolution of the tomography applied to the sample. The two largest pore size ranges, centered in 40 and 300 μm, have to be accurately modeled. As shown in Fig. 2b, a spatial resolution close to 5 μm associated with a size parameter $D/a = 8$ for the 40 μm pores, corresponds to an acceptable accuracy of 5×10^{-2}.

In practice, the intensity matrix of this real porous medium has been obtained by X-ray tomography [27,28] at ESRF (line ID19), Grenoble, France with a spatial resolution a of 4.9 μm. The required storage volume for the whole sample corresponds to about 8×10^9 voxels, i.e. 8 Gb.

4.2. Implementation of the Monte Carlo approach

In order to calculate G_e, G_a and $p_v(\mu_s)$, a Monte Carlo technique has been used, based on a huge number of rays, issued from random source points M in the whole porous medium, typically 10^9. The first step consists to choose a ray unit vector $\mathbf{u_k}$ and a point M in the shooting volume of the sample, i.e. a representative volume of the sample from which rays are issued.

If M is in the fluid phase, extinction only occurs in a point I of the interface. The marching cube algorithm, which allows us to determine Σ_t, is based on a moving cube of 8 adjacent voxels generated around the current discretized abscissis s_i from M along the followed ray. If, at a given step, the marching cube contains a part of the interface Σ_t the existence of any intersection with the ray will be checked by an algorithm. If there is no intersection a new marching cube is defined around the following abscissis s_{i+1}. In case of intersection, the first impact point I is determined and the extinction distance MI is a contribution to G_e, as shown in Eq. (7). The normal unit vector to the interface $\mathbf{n}$ at the point I is defined and the different contributions to the phase function are obtained as explained in Section 2.3, by using equations similar to Eq. (14).

If M is in the semi-transparent solid phase, of extinction coefficient β_S, an extinction length $d_S = -\ln(\xi_1)/\beta_S$ is deduced from a random number ξ_1 generated in the range $[0,1]$. The same algorithm as in the fluid phase is then used to determine an interfacial extinction distance MI. If there is a point I of the interface such as $MI < d_S$ the previous procedure is applied. If not, d_S is also a contribution to G_e. In this case, a second random number ξ_2 is generated in the range $[0,1]$. If ξ_2 is smaller than κ_S the ray is assumed absorbed; d_S is then contribution to G_a, as shown in Eq. (10). If ξ_2 is higher than κ_S the ray is scattered; the two scattering angles defining the unit vector $\mathbf{u}_s$, are obtained from the scattering phase function of the solid phase by classically generating two associated random numbers.

4.3. Results

In order to check the statistical homogeneity of the results, the mullite sample defined in Section 4.1 has been divided into three cylindrical shooting volumes called A, B and C shown in Fig. 4a; each of them is characterized by a 6 mm diameter and 2 mm height. The distance between a shooting volume border and the sample border has been chosen at less two times higher than the 1 mm previously estimated length, in order to avoid artefacts due to the degradation of the structure in the vicinity of the sample border. It is also worth noticing that the size of a shooting volume has been chosen larger than the cumulated size of 1000 cubic shooting volumes in use in Ref. [20]. This choice allows us to obtain statistically representative results.

In order to take into account the statistical anisotropy of β_v and κ_v, Monte Carlo calculations have been carried out for 400 solid angles $\Delta\Omega$ centered in the directions defined

by the angles θ and ϕ defined in Fig. 4b. The θ and ϕ angles have been incremented in such a way to uniformly cover 4π steradians, i.e. with $\Delta\cos(\theta_i) = 1/10$ and $\Delta\Phi_i = \pi/10$. The number of generated rays is equal to 2.5×10^6 per solid angle. At this limit, the obvious symmetry condition $\beta_v(\theta,\phi) = \beta_v(\pi - \theta, \pi + \phi)$ has been checked.

Two levels of calculations have been carried out due to the huge memory capacity required by all the 8×10^9 voxels defining the sample and the huge required computational time, especially for the phase function. A complete directional study has been first achieved with a downgraded spatial resolution $a' = 19.6$ μm, equal to 4 times the tomography resolution. In these conditions, the D/a parameter defined in Section 3 is equal to 15 for the largest pore size, which leads to a typical accuracy criterion of 10^{-3}, but only equal to 2 for the middle size pores, which does not theoretically lead to a sufficient accuracy criterion. In a second step, a limited number of calculations with a spatial resolution of 4.9 μm have been carried out for a limited number of directions.

With the downgraded spatial resolution, the results related to β_v and κ_v vs θ and ϕ, averaged by using the three shooting volumes A, B and C, have been first considered. A typical example of identification of G_e and g_e is given in Fig. 5. Due to the cutoff related to the medium size pore distribution, G_e is not continuous, for intermediate optical thicknesses. The relative standard deviation σ_{MC}, associated with the calculation of $G_e(\theta,\phi)$ and defined by Eq. (15) is in the range $[3.53 \times 10^{-4}, 8 \times 10^{-4}]$. Results related to the 400 directions are shown in Fig. 6a and c for β_v and κ_v, respectively. The relative error function $\varepsilon_e(\beta_v)$, associated with the determination of β_v by identification of G_e and g_e and defined by Eq. (9), is in the range [0.03, 0.045], as shown in Fig. 6b and will be discussed later. This error criterion is important in practice for radiative heat transfer calculations insofar as G_e is a transmissivity in use in such discretized calculations. A simple representation of the results is given by the dependence of the directional extinction length $l = 1/\beta$ vs θ and ϕ. This quantity is accurately fitted by the ellipsoid $(x^2/l_x^2 + y^2/l_y^2 + z^2/l_z^2 = 1)$ where l_x, l_y and l_z are the extinction lengths associated with the three principal axes Ox, Oy, Oz of the ellipsoid, equal to 0.195, 0.231, 0.208 mm, respectively. The relative least square error due to the identification by the ellipsoid from original β_v data is 3.3×10^{-5}. The angle between the principal axis of the ellipsoid Oz and the axis OZ of the sample defined in Fig. 4b is equal to 3°. This angle could simply come from the inclination of the sample on the optical setup at ESRF. It is worth of notice that the error associated with the identification of the results with an ellipsoid is much smaller than the error $\epsilon_e(\beta_v)$ associated with the identification of G_e and g_e and can be here neglected.

The statistical homogeneity of the sample has been established by considering, for the three axes of the ellipsoid, the relative standard deviations $\sigma_{\beta_{vi}}/\bar{\beta}_{vi}$ $(i = x, y, z)$ corresponding to three independent treatments of the shooting volumes A, B and C with the downgraded spatial resolution. These relative standard deviations less than

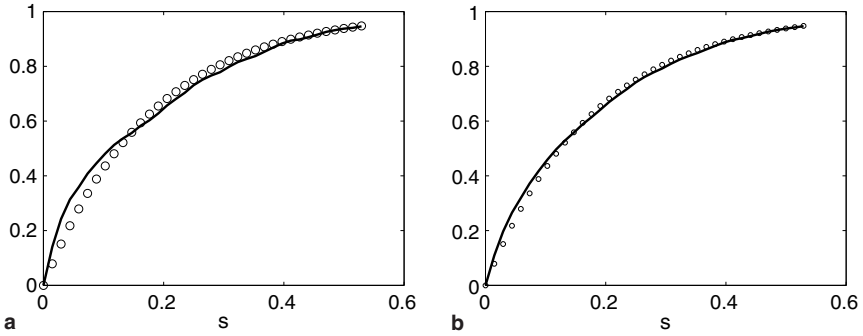

Fig. 5. Example of identification of $G_e(s)$ (solid line) and $g_e(s)$ (circles); (a) downgraded spatial resolution ($a' = 19.6$ μm) ; (b) high spatial resolution ($a = 4.9$ μm).

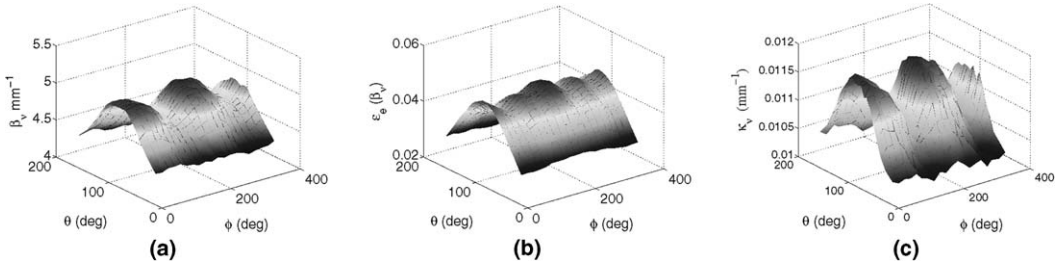

Fig. 6. (a) Identified directional extinction coefficient β_v for the 0.6328 μm wavelength and $a' = 19.6$ μm. (b) Directional identification error $\epsilon_e(\beta_v)$. (c) Identified directional absorption coefficient κ_v for the 0.6328 μm wavelength and $a' = 19.6$ μm.

0.016 are smaller than the identification error $\epsilon_e(\beta_{vi})$ in the range 0.034–0.042. The sample can be considered as statistically homogeneous.

It also appears that the discrepancies between the mean value of $\bar{\beta}_{vx}$ and $\bar{\beta}_{vy}$, 5.13 and 4.81 mm^{-1}, respectively are of the same order of magnitude as the typical absolute error 0.2 mm^{-1} associated with $\epsilon_e(\beta_v)$, error important for any radiative heat transfer calculation. On the other hand, the discrepancies between $\bar{\beta}_{vz}$ (equal to 4.33 mm^{-1}) and $\bar{\beta}_{vx}$ or $\bar{\beta}_{vy}$ are typically of about 0.7 mm^{-1}, i.e. at least three times larger than the previous typical error. In a first approach, the field of β_v can be considered as axisymmetric around axis Oz. A limited number of calculations have been carried out for the ultimate tomography results ($a = 4.9$ μm), for only the shooting volume A and the three principal directions of the previously obtained ellipsoid x, y and z. Only 10^5 rays have been generated for each direction in this case. It is worth of notice in Fig. 5b that the obtained G_e function is more continuous than previously for intermediate optical thicknesses. But due to weak number of generated rays, 25 times weaker than previously, the standard deviation associated with G_e is in the range $[10^{-3}, 2\times10^{-3}]$. Table 1 shows the results β_{vih} obtained with the high spatial resolution for the principal axis x, y and z, compared to those obtained with the low resolution. It is shown that: (i) the identification error in the β_{vih} determination $\epsilon(\beta_v)$ is similar to the previous corresponding error, despite of the weak number of rays; (ii) the relative discrepancy between the values of β_{vih} obtained with the two spatial resolutions are less than 2% for the three directions. In these conditions, the results obtained with the downgraded resolution can be considered as representative.

Table 1
Comparison of the two levels of β identification

	x	y	z
β_{vhi} (mm^{-1})	5.03	4.75	4.28
$\epsilon_{eh}(\beta_v)$	0.038	0.035	0.031
β_{vli} (mm^{-1})	5.13	4.81	4.33
$\epsilon_{el}(\beta_v)$	0.042	0.038	0.034
ϵ_r	0.0195	0.0121	0.0118

The index h is associated to the high spatial resolution $a = 4.9$ μm; l to the low spatial resolution $a = 19.6$ μm; $\epsilon_r = (\beta_{vhi} - \beta_{vli})/\beta_{vhi}$.

It is also worth of notice that the tomographed sample has been correctly defined. In fact the chosen 1 mm critical length s_c corresponds to an optical extinction thickness of 4.3, which is a value larger than the cutoff of 3 used in our approach. The determined directional absorption coefficients κ_v are shown in Fig. 6c. Depending on the direction, κ_v varies in the range $[0.01, 0.0115]$ mm^{-1}. A typical value of the albedo ω is about 0.999.

At this step, it is worth noticing that the identification of β_v and κ_v have been also carried out under the arbitrary assumption that the medium is statistically isotropic, by determining the corresponding isotropic values of these quantities. The interesting fact is that the identification error is then of the same order than the one associated with the anisotropic assumption. This fact enhances a limitation of the identification methods based on too simplified models. The identified phase function defined in Eq. (14) only depends, in practice, on the cosine of the scattering angle $\mu_s = \mathbf{u}\cdot\mathbf{u}'$ as shown in Fig. 7a and b. Indeed, the standard deviation $\sigma(\mu_s)$ shown in Fig. 7b, associated with the 400 considered directions is much smaller than $p(\mu_s)$ for any μ_s value. Contrary to the cases of β_v and κ_v, p_v does not depend on the current direction $\mathbf{u}$. In practice, this phase function is isotropic for μ_s smaller than 0.75 and exhibits a sharp maximum in the forward direction.

5. Conclusion

We have associated with the porous considered material a unique equivalent semi-transparent medium. The directional extinction and absorption coefficients of this medium have been determined from both tomography discretized data and the radiative properties of the semi transparent solid phase. The phase function of the equivalent medium, which only depends on the scattering angle, has also be determined.

All these results have been compared to experimental results and validated in Ref. [26]. Indeed, the data obtained in the present work have been used in a Monte Carlo transfer model in order to directly calculate the bidirectional reflectance of the sample vs three incident angles. Relative discrepancies between calculated reflectance and

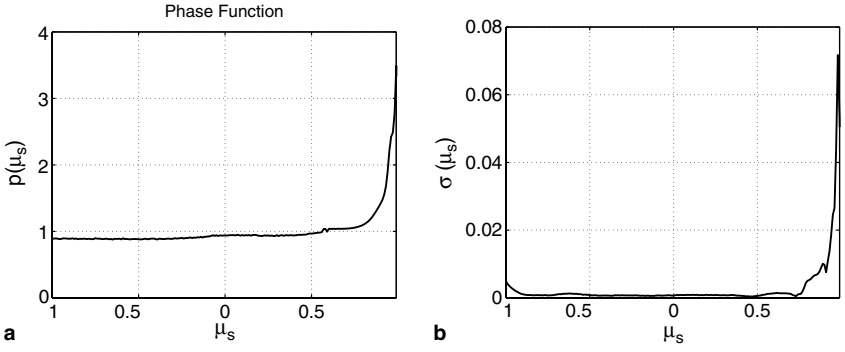

Fig. 7. (a) Directional phase function $\overline{p(\mu_s)}$ averaged on the 400 incident directions; $\lambda = 0.6328$ μm; $a' = 19.6$ μm. (b) Standard deviation over $p(\mu_s)$.

measurements are only of a few per cent. It is a first validation case of the RDFI method.

Acknowledgements

The authors thank D. Rochais and F. Enguehard from CEA Le Ripault (Tours, France) for the mercury porosimetry measurements, J. Vicente from IUSTI (Marseille, France) for the material visualization and P. Echegut from CRMHT (Orléans, France) for helpful discussions.

References

[1] Y. Yang, J. Howell, D. Klein, Radiative heat transfer through a randomly packed bed of spheres by the Monte Carlo method, J. Heat Transfer 105 (1983) 325–332.
[2] C. Argento, D. Bouvard, A ray tracing method for evaluating the radiative heat transfer in porous media, Int. J. Heat Mass Transfer 39 (15) (1996) 3175–3180.
[3] S. Subramaniam, M. Mengüc, Solution of the inverse radiation problem for inhomogeneous and anisotropically scattering media using a Monte Carlo technique, Int. J. Heat Mass Transfer 34 (1) (1991) 253–266.
[4] B.P. Singh, M. Kaviany, Independent theory versus direct simulation of radiation heat transfer in packed beds, Int. J. Heat Mass Transfer 34 (11) (1991) 2869–2882.
[5] B.P. Singh, M. Kaviany, Modelling radiative heat transfer in packed beds, Int. J. Heat Mass Transfer 35 (6) (1992) 1397–1405.
[6] X. Fu, R. Viskanta, J.P. Gore, A model for the volumetric radiation characteristics of cellular ceramics, Int. Commun. Heat Mass Transfer 24 (8) (1997) 1069–1082.
[7] C. Coquard, D. Baillis, Radiative characteristics of opaque spherical particle beds: a new method of prediction, AIAA J. Thermophys. Heat Transfer 18 (2) (2004) 178–186.
[8] R. Coquard, D. Baillis, Radiative characteristics of beds of spheres containing an absorbing and scattering medium, J Thermophys. Heat Transfer 19 (2) (2005) 226–234.
[9] R. Coquard, D. Baillis, Radiative characteristics of beds made of large spheres containing an absorbing and scattering medium, Int. J. Thermal Sci. 44 (2005) 926–932.
[10] Q. Brewster, Volume scattering of radiation in packed beds of large opaque spheres, Trans. ASME 126 (2004) 1048–1050.
[11] L. Glicksman, M. Shuetz, M. Sinofsky, Radiation heat transfer in foam insulation, Int. J. Heat Mass Transfer 30 (1) (1987) 187–197.
[12] T.J. Hendricks, J.R. Howell, Inverse radiative analysis to determine spectral radiative properties using the discrete ordinates method, in: G.F. Hewitt (Ed.), The Tenth International Heat Transfer Conference, vol. 2, Taylor and Francis, Brighton, UK, 1994, pp. 75–80.
[13] T.J. Hendricks, J.R. Howell, Absorption/scattering coefficients and scattering phase function in reticulated porous ceramics, ASME J. Heat Transfer 118 (1) (1996) 79–87.
[14] T.J. Hendricks, J.R. Howell, New radiative analysis approach for reticulated porous ceramics using discrete ordinates method, ASME J. Heat Transfer 118 (4) (1996) 911–917.
[15] D. Doermann, J.F. Sacadura, Heat transfer in open cell foam insulation, ASME J. Heat Transfer 118 (1996) 88–93.
[16] D. Baillis, M. Raynaud, J.F. Sacadura, Spectral radiative properties of open-cell foam insulation, J. Thermophys. Heat Transfer 13 (3) (1999) 292–298.
[17] R. Lopes, M. Luis, D. Baillis, J.F. Sacadura, Directional spectral emittance of a packed bed: correlation between theoretical prediction and experimental data, ASME J. Heat Transfer 123 (2001) 240–248.
[18] D. Baillis, J.F. Sacadura, Identification of polyurethane foam radiative properties-influence of transmittance measurements number, J. Thermophys. Heat Transfer 16 (2) (2002) 200–206.
[19] D. Baillis, J.F. Sacadura, Thermal radiation properties of dispersed media: theoretical prediction and experimental characterization, JQSRT 67 (5) (2000) 327–363.
[20] M. Tancrez, J. Taine, Direct identification of absorption and scattering coefficients and phase function of a porous medium by a Monte Carlo technique, Int. J. Heat Mass Transfer 47 (2) (2004) 373–383.
[21] R. Siegel, J. Howell, Thermal Radiation Heat Transfer, fourth ed., Taylor and Francis-Hemispher, Washington, 2001.
[22] M. Born, E. Wolf, Principle of Optics—X-ray Tomography in Material Science, seventh ed., Pergamon Press, 1999.
[23] B. Zeghondy, Caractérisation des propriétés radiatives anisotropes d'un matériau poreux par identification de fonctions de distribution radiatives; validation expérimentale, Thèse de Doctorat, École Centrale Paris, Chatenay Malabry, 2005.
[24] J.-F. Delesse, Diffusion et réaction des gaz en milieux poreux, Thèse de Doctorat, Université Bordeaux I, 2002.
[25] K. Michielsen, H. De Raedt, Integral-geometry morphological image analysis, Tech. rep., Laboratory for Biophysical Chemestry, University of Groningen, Nijenborgh 4, 9747 AG Groningen, Netherlands, 2001.
[26] B. Zeghondy, E. Iacona, J. Taine, Experimental validation of RDFI method predictions of statistically anisotropic porous medium radiative properties, Int. J. Heat Mass Transfer, in press.
[27] G.T. Herman, Image Reconstruction from Projections—the Fundamentals of Computerized Tomography, Werner Rheinboldt, 1980.
[28] J. Baruchel, J.Y. Buffière, E. Maire, P. Merle, G. Peix, X-ray Tomography in Material Science, HERMES Science Publications, 2000.